Iron species incorporated over different silica supports for the heterogeneous photo-Fenton oxidation of phenol

F. Martínez*, G. Calleja, J. A. Melero and R. Molina

Department of Chemical and Environmental Technology

ESCET. Rey Juan Carlos University.

C/ Tulipán s/n, 28933. Móstoles, Madrid

Spain

* Corresponding author

Phone: 34 91 488 7182

Fax: 34 91 488 70 68

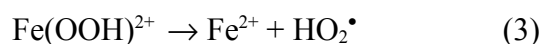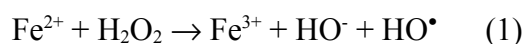E-mail: fernando.castillejo@urjc.es (F. Martínez)

Abstract

Iron-containing catalysts have been prepared following different synthesis routes and silica supports (amorphous, zeolitic and mesostructured materials). Activity and stability of these materials were assessed on the photo-Fenton degradation of phenolic aqueous solutions using near UV irradiation (higher than 313 nm) at room temperature and initial neutral pH. Their catalytic performance was monitored in terms of phenol and total organic carbon (TOC) conversions. Aromatic compounds and carboxylic acids as by-products coming from incomplete mineralization of phenol as well as the efficiency of each catalytic system in the use of the oxidant were also studied. Stability of the materials throughout the photo-Fenton reaction was evaluated in terms of metal leachibility. Activity and stability depend on the environment of iron species and features of silica support. The evolution of pH with the reaction time and their relationship with TOC degradation and leaching degree has been discussed. A nanocomposite material of crystalline iron oxides supported over mesostructured SBA-15 material is shown the most successful catalyst for degradation of phenolic aqueous solutions by photo-Fenton processes, achieving an outstanding overall catalytic performance accompanied with a noteworthy stability.

1. INTRODUCTION

The effective removal of aromatic pollutants present in wastewater streams generated by industrial processes has become a challenge task due to a more restrictive environmental laws and regulations. Aromatic compounds are refractory to conventional chemical and biological treatments, and this is the reason why other methods are being studied [1-2]. Advanced Oxidation Processes (AOP's) have emerged as interesting alternative for the destruction of organic pollutants in industrial wastewater. These processes basically involve the generation of reactive hydroxyl radicals (OH$^\bullet$) with high oxidation potential, which are able to mineralize these refractory compounds [3]. Fenton's reagent as oxidation system based on the reaction of H_2O_2 with Fe(II)/Fe(III) ions has been used as a powerful source of oxidative radicals [4-5]. It is generally accepted the generation of hydroxyl radicals by the reaction of H_2O_2 with ferrous ions, whereas Fe (III) reacts with H_2O_2 leading to the regeneration of Fe (II), extending the Fenton process [6]:

$$Fe^{2+} + H_2O_2 \rightarrow Fe^{3+} + HO^- + HO^\bullet \quad (1)$$

$$Fe^{3+} + H_2O_2 \leftrightarrow Fe(OOH)^{2+} + H^+ \quad (2)$$

$$Fe(OOH)^{2+} \rightarrow Fe^{2+} + HO_2^\bullet \quad (3)$$

The generation of hydroxyl radicals can be enhanced by UV radiation due to the photoreduction of hydroxilated Fe (III) ions or ferrihydroxalate ($Fe(III)(OH)^{2+}$) in aqueous solution promoting an additional production of $HO^{\bullet}$ radicals [7]:

$$Fe(III)(OH)^{2+} + h\nu \rightarrow Fe^{2+} + HO^{\bullet} \qquad (4)$$
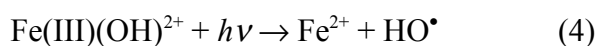
The use of the Fenton's reagent as homogeneous catalyst implies several drawbacks. A limited range of pH (2.5-3.5) has to be used so that the reaction takes place. In a second term, recovery of iron ions from the solution through additional separation steps is needed in homogeneous catalytic systems to comply with environmental regulations. In this sense, a challenging issue is the immobilization of iron species over different supports as catalyst for photo-Fenton processes which would also enable its application under non-controlled pH conditions. Y zeolite-exchanged iron (III) has been used for the degradation of 2,4-xylidine in a bench photochemical reactor and in a solar reactor [8], obtaining interesting results in terms of pollutant elimination and leaching degree, but pH around of 3 was necessary. Iron (II)-containing 13X zeolite has been tested in the photo-enhanced Fenton degradation of low concentrated phenolic aqueous solutions (100 ppm) [9]. A low exchange of iron species within the zeolitic framework and its poor stability are shown as the major drawbacks of this material. Nanosized Fe_2O_3 particle oxides intercalated as pillars between layered clays such as laponite and bentonite have revealed a high photocatalytic activity for discoloration and mineralization of different dyes using a high energetic 254 nm UV irradiation [10, 11]. Similar works have been also described for the degradation of different azo-dyes over iron oxides such as goethite and hematite under non-controlled pH conditions [12].

Nafion, as films or pellets, has been employed as organic support due to the presence of sulphonic groups allowing the effective anchoring of Fe ions [13]. However, Nafion materials show a low photocatalytic activity and are not very attractive due to their relative high cost. Finally, a novel Fe/C structured fabric has been successfully used for the complete discoloration of Orange II, but a high hydrogen peroxide to substrate ratio was needed [14].

The main purpose of this work is to assess the catalytic performance of different silica-supported iron systems taking into account their activity and stability in photo-assisted Fenton processes. Several materials such as crystalline iron oxides supported over amorphous and mesostructured silica materials as well as isolated iron species isomorphously substituted within SBA-15, zeolitic silicalite-1 and amorphous silica frameworks have been prepared, characterized and tested in the degradation of phenolic aqueous solutions. UV irradiation near visible (> 313 nm) has been used which represents a significant advantage for future application in solar photodegradation processes. Likewise, all the reactions were carried out with a hydrogen peroxide concentration close to the stoichiometric amount necessary for complete mineralization of the initial phenol content. The catalytic performance has been determined in terms of phenol and total organic carbon (TOC) conversions, whereas other parameters such as the efficient use of the oxidant, distribution of intermediates, pH during reaction and iron resistance to leaching out into the aqueous solution were thoroughly studied.

2. EXPERIMENTAL

2.1 Catalysts preparation

Iron-containing SBA-15 material (D-1 sample) was prepared using a direct synthesis procedure described elsewhere [15]. This route involves the co-condensation of iron and silica sources (FeCl$_3$·6H$_2$O and tetraethoxysilicate, TEOS; Aldrich) under acidic conditions and templated with Pluronic 123 followed with an ageing step of the mixture at 110ºC during 24 hours under static conditions. The procedure was slightly modified changing the ageing pH to 3.5 (D-2 sample) and 7 (D-3 sample) by addition of an appropriate amount of ammonia aqueous solution with the purpose of increasing the incorporation of iron species by partial precipitation of non-soluble iron oxy-hydroxides. After ageing step, the solids were recovered by filtration and air dried at room temperature overnight. Crystallization of iron oxy-hydroxides and template removal are carried out by calcination in air at 550ºC for 5 hours.

Amorphous SiO$_2$-Fe$_2$O$_3$ mixed oxide (AM sample) was prepared following a two step sol-gel process [16], consisting of a first acid-catalyzed hydrolysis step of the iron and silica sources, followed with a basic condensation with an aqueous tetrapropylammonium hydroxide solution (20 wt. % TPAOH, Alfa). The resultant solid was dried overnight at 110 ºC and calcined in air at 550ºC during 5 hours. The solid was prepared with an initial SiO$_2$/Fe$_2$O$_3$ molar ratio of 155.

Iron-containing zeolitic material (ZM sample) was synthesized by hydrothermal treatment of a wetness impregnated SiO$_2$-Fe$_2$O$_3$ mixed oxide with an aqueous 20 wt. % TPAOH solution (1.6 g of TPAOH solution per 1 g of dried cogel). The crystallization

of the material was carried out in a teflon-lined autoclave under autogenous pressure and static conditions at 170 °C for 3 hours [17]. The solid after synthesis was separated by centrifugation, washed several times with distilled water, dried overnight at 110 °C and finally calcined in air at 550 °C for 5 hours.

Commercial hematite with a BET surface area of 60 m^2/g was purchased from Aldrich with the purpose of comparison.

2.2 Catalyst characterization

X-ray powder diffraction (XRD) data were acquired on a Philips X-Pert diffractometer using Cu Kα radiation. Data were collected from 2θ ranging from 0.5 to 90° with a resolution of 0.02°. Nitrogen adsorption and desorption isotherms at 77 K were measured using a Micromeritics Tristar 3000 System. Transmission electron microscopy (TEM) microphotographs and energy-dispersive X-ray (EDX) microanalysis were carried out on a PHILIPS TECNAI-20 electron microscope operating at 200 kV. Bulk iron content of the synthesised samples was performed by means of Atomic Emission Spectroscopy with Induced Coupled Plasma (ICP-AES) analysis collected in a Varian Vista AX system.

2.3 Photo-Fenton reactions

Heterogeneous photo-Fenton reactions were carried out in a Pyrex batch cylindrical magnetically stirred reactor containing 1 L of the aqueous dispersion of the catalyst and

the pollutant. The irradiation was performed with a 150W medium pressure mercury lamp (Heraeus TQ-150) inside a quartz jacket, immersed in the mixture and coaxial with the photoreactor. The lamp was surrounded by a cooling tube in which a copper sulphate aqueous solution was circulating to refrigerate the suspension and cutting off radiation with a wavelength shorter than about 313 nm. The temperature was maintained at 25 ºC.

In a typical photo-catalytic run the appropriate amount of catalyst (0.5 g/L) was dispersed in 980 mL of distilled water and introduced into the reactor. The lamp was immersed in the reactor and switched on during 15 minutes before adding both phenol and hydrogen peroxide, in order to avoid the inherent induction time of the irradiation source. Thereafter, a small volume of high-concentrated aqueous solution of phenol with the required amount of hydrogen peroxide was added to the reactor up to obtain 1L of aqueous solution. Initial reaction conditions were 0.5 g/L of phenol (corresponding to 380 ppm of total organic carbon - TOC) and 2450 ppm of hydrogen peroxide (corresponding to 95 % of stoichiometric oxidant concentration required for the complete mineralization of phenol, according to reaction 5). The pH of the reaction medium was not buffered, being the initial value around 6.

$$C_6H_6O + 14\ H_2O_2 \rightarrow 6CO_2 + 17\ H_2O \qquad\qquad (5)$$
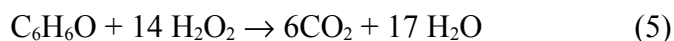
Aliquots of 8-10 ml were taken at 30, 75, 150 and 240 minutes during the reaction course. High performance liquid chromatograph (HPLC) model Varian Prostar was equipped with a Waters Spherisorb column (4.6 x 150 mm) and an UV detector at 215

nm. A mixture of methanol (20 vol. %) and water (80 vol. %) buffered at pH=2.6 was used as mobile phase. HPLC analysis was used for the quantitative determination of phenol and by-products coming from its incomplete mineralization (hydroquinone and catechol as aromatic compounds; formic, acetic and maleic as carboxylic acids). Other oxygenated compounds were not measured by HPLC analysis due to interferences with remaining hydrogen peroxide. Residual total organic carbon (TOC) content of the solutions after reaction was analysed using a combustion/non dispersive infrared gas analyser model TOC-V Shimadzu. The contribution of different degradation products in the residual TOC in terms of carbon percentage was calculated as follows:

$$\text{Aromatics} (C^A) = \frac{\text{ppm of C coming from aromatic compounds measured by HPLC}}{\text{Residual TOC (ppm of C)}} \times 100$$

$$\text{Carboxylic acids} (C^{CA}) = \frac{\text{ppm of C coming from carboxylic acids measured by HPLC}}{\text{Residual TOC (ppm of C)}} \times 100$$

$$\text{Rest of oxygenated compounds} (C^{OO}) = 100 - C^A - C^{CA}$$

Peroxide concentration after reaction was evaluated by iodometric titration. The efficiency of the oxidant use was defined as:

$$\text{Efficiency} = \frac{\text{TOC conversion (\%)}}{\text{Oxidant conversion (\%)}}$$

Iron content in the filtered solution after reaction was measured by ICP-AES analysis collected in a Varian VISTA AX system.

3. RESULTS AND DISCUSSION

3.1 Catalysts properties

Table 1 lists physicochemical and textural properties as well as iron content of all calcined samples.

Table 1. Physicochemical properties of different Fe-containing materials

| Samples | Type of material | XRD | | Fe content[c] (% wt) | S_{BET}[d] (m^2/g) | D_p[e] (Å) |
		Low Angle Order[a]	High Angle Order[b]			
D-1	Fe-SBA-15	Yes	No	1.2	715	86
D-2	Crystalline Oxide/SBA-15	Yes	Yes	16.0	468	68
D-3	Crystalline Oxide/SiO_2	No	Yes	22.0	315	-[f]
AM	Mixed SiO_2/Fe_2O_3 oxide	No	No	1.2	872	30
ZM	Fe-Silicalite	No	Yes	1.2	423	5.5
Hematite	Crystalline Fe_2O_3	No	Yes	-	60	-

[a] Used to determine 2-D hexagonal arrangements in mesoporous materials
[b] Used to determine crystalline structures (zeolitic framework or iron oxide phases)
[c] Determined by ICP over the bulk powder sample
[d] Specific surface area
[e] Mean pore size
[f] Broad pore size distribution

XRD spectra depicted in Figure 1 and summarized in Table 1 show the different siliceous structure and crystalline phases for the synthesized materials. It can be easily inferred that the increase of pH during ageing of iron-containing SBA-15 materials

promotes the appearance of crystalline oxide entities with a gradual disappearance of typical 2-D hexagonal arrangement of mesoporous SBA-15 material and decreasing of the specific surface area (samples D-1, D-2 and D-3). Note that D-3 sample evidences a complete absence of mesoscopic order and a low surface area. Additionally, AM sample displays an XRD pattern corresponding to amorphous materials which is completely converted into a zeolitic solid with a typical MFI framework after hydrothermal treatment (ZM sample).
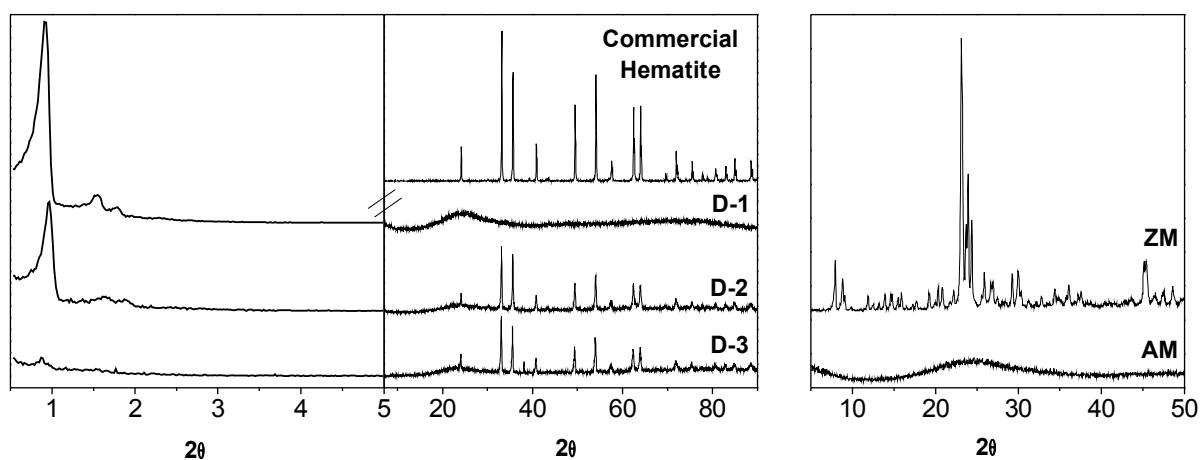
Figure 1. XRD spectra of iron-containing materials

TEM micrographs (Figure 2) confirm the presence of crystalline oxides embedded within the structure of D-2 and D-3 samples, and their absence for D-1 sample. Microanalysis measurements confirm the homogeneity of Fe content in the highly mesostructured material (D-1 sample), which agree with the metal concentration determined by ICP-AES over the bulk powder sample. D-2 sample shows zones with a high concentration of Fe which are related to the presence of crystalline iron oxide particles and areas with low contents (ca. 3.6 %) for the well-ordered channels characteristic of SBA-15 materials. Finally, D-3 sample predominantly displays the presence of microaggregates of hematite.
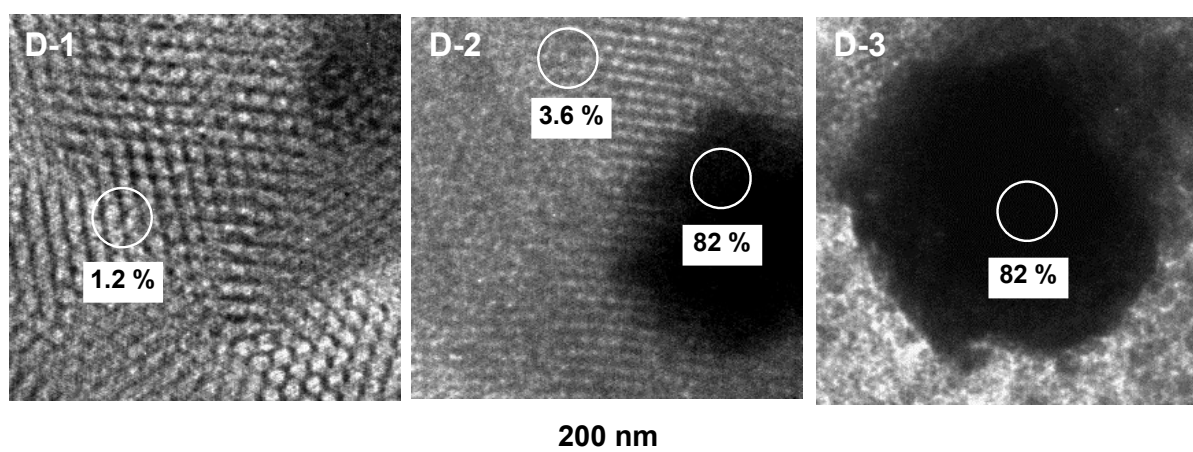
Figure 2. TEM images of D-1, D-2 and D-3 samples. Numbers indicate the percentage of iron in wt. % measured by EDX microanalysis

In previous works [17, 18] the analysis of local iron environment in these materials has been studied by means of Mössbauer spectroscopy. In strong acidic media (D-1) iron is incorporated into the SBA-15 structure in ionic dispersion. Samples aged in moderately acidic conditions (pH ~3.5, D-2) or neutral media (D-3) are composite materials and they contain crystalline iron oxide particles embedded into the mesostructured matrix in a wide distribution of size (30 – 300 nm). At neutral pH, mostly regular hematite is formed whereas ageing in mild acidic media leads to more disordered iron oxide phases [18]. In particular for D-2 sample, a small part of iron is even present in ionic dispersion into the siliceous matrix. In concern to the other two materials, mixed SiO_2-Fe_2O_3 oxide is mainly constituted of $(Si\text{-}O\text{-})_n Fe(OH)_{(4-n)}$ units resulting from the sol-gel process used for the preparation of this material with iron in isolated positions within the amorphous silica framework [19]. Finally, iron species in Fe-silicalite are in framework positions isomorphously substituted within the MFI structure. Table 2 summarizes the contribution of different iron environments obtained

from Mössbauer studies for the synthesized materials (see references 17 and 18 for experimental details).

Table 2. Environment of iron species incorporated within the different synthesized materials

Iron species	D-1	D-2	D-3	AM	ZM
Isolated ionic iron species (%)	100	13	10	100	100
Disordered iron oxide phases (%)	-	45	-	-	-
Hematite crystalline particles (%)	-	42	90	-	-

3.2 Activity and stability of catalytic systems in photo-assisted oxidation of phenolic aqueous solutions

Table 3 summarizes the activity of all the catalysts prepared during this study in the photo-Fenton process in terms of TOC and phenol degradation at different reaction times. A nearly total phenol removal is displayed by D-1, D-2, D-3 and AM samples after reaction times of 240 minutes. Comparing values of TOC degradation for catalysts with similar content and nature of iron species (D-1, AM and ZM samples), a low activity of zeolitic material is clearly seen. Intraparticle diffusion problems arising from the limited pore size of the Fe-silicalite could hinder the access of organic molecules to metallic active sites. High iron-containing catalysts consisting of crystalline iron oxide particles as active species (D-2, D-3 samples and pure iron oxide as hematite) exhibit distinct TOC degradation rates. It must be pointed out the outstanding activity of D-2 sample, based on crystalline iron oxides supported over mesostructured SBA-15, in

contrast to D-3 sample with mostly hematite as crystalline iron oxide embedded into amorphous silica network or commercial and unsupported hematite.

Table 3. Experimental results of the photo-Fenton oxidation of phenol over iron-containing materials

Sample	t_r (min)	X_{TOC} (%)	X_{Phenol} (%)	Leaching (%)[a]
D-1	15	0.0	87.8	7.3
	30	2.5	87.0	10.0
	75	16.6	95.0	23.2
	150	22.4	98.0	29.2
	240	29.2	98.8	34.0
D-2	15	13.9	60.0	0.5
	30	35.9	85.2	0.7
	75	39.7	94.8	1.1
	150	44.5	99.6	1.4
	240	48.1	99.6	1.7
D-3	15	0.0	20.0	0.1
	30	3.7	63.2	0.5
	75	12.2	86.8	0.7
	150	13.8	93.2	0.9
	240	19.1	96.6	1.0
AM	15	5.2	40.0	3.9
	30	10.0	75.6	16.7
	75	25.3	95.4	25.8
	150	29.6	97.8	29.2
	240	37.0	98.6	31.7
ZM	15	0.0	30.0	≤ 0.01
	30	5.3	44.0	≤ 0.01
	75	9.9	56.8	≤ 0.01
	150	12.3	64.0	≤ 0.01
	240	15.4	68.8	≤ 0.01
Commercial Hematite	15	0.0	4.0	≤ 0.01
	30	0.0	20.4	≤ 0.01
	75	2.1	26.4	≤ 0.01
	150	3.6	34.0	≤ 0.01
	240	5.5	37.0	≤ 0.01

[a] Percentage of iron leached from the catalyst

D-2 material yielded ca. 48 % of TOC removal and the complete degradation of aromatics compounds after 240 minutes of reaction. It has been demonstrated that the

photo-activity of a catalyst can be influenced by its surface area, crystal structure, particle size distribution or surface hydroxyl group density [20]. In this sense, the physicochemical properties of mesostructured SBA-15 phase as support for the immobilization of crystalline iron oxides allows to enhance the catalytic performance of D-2 material, probably due to the improvement of the typical requirements of a photocatalyst such as a high light absorption and efficient quantum yield in the production of excited compounds and radical species which are responsible of the degradation of organic matter.

Catalytic activity of the different catalysts was also explored taking into account the distribution of by-products coming from the partial oxidation of phenol. The contribution of aromatic compounds, carboxylic acids and other oxygenated products on the remaining TOC concentration after 240 minutes of reaction is depicted in Figure 3.
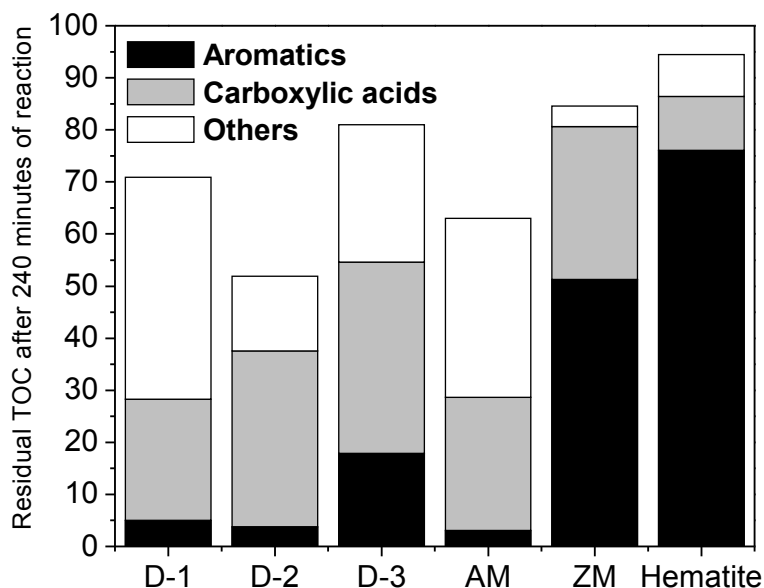
Figure 3. Residual TOC and contribution of by-products in the photo-catalytic degradation of phenol for different iron-containing materials

As expected, samples with low TOC conversion (ZM and commercial hematite) evidence a high aromatic content, whereas those materials with higher values of TOC removal (D-2, AM and D-1 samples) exhibit an almost complete degradation of this kind of compounds. Unlike to the other catalytic systems in which the contribution of aromatics or other oxygenated intermediates is dominant over the remaining TOC concentration, D-2 sample shows a relevant fraction of the TOC concentration for low molecular weight carboxylic acids. These results could account for the above commented better catalytic performance of D-2 catalyst which yields an easy degradation of aromatic and oxygenated intermediates towards final refractory compounds such as formic, acetic or maleic acids.

An important point in the design of heterogeneous catalytic systems for advanced oxidation processes is the resistance of metal species to be leached into the aqueous solution under the oxidant and acidic conditions in which Fenton reactions usually proceed. In this sense, stability of all the materials was evaluated in terms of the percentage of iron leached from the catalyst with the reaction time, being the results summarized in Table 3. D-1 sample evidences a high leaching degree in comparison to those obtained for D-2 and D-3 samples, which are mainly composed of supported crystalline iron oxide species. These crystalline oxide species seem to be extremely resistant to be leaching out into the aqueous solution. Amorphous Fe_2O_3-SiO_2 mixed oxide (AM sample) exhibits a loss of iron species similar to D-1 sample. Crystallisation of the amorphous Fe_2O_3-SiO_2 into a zeolitic framework (ZM sample) induces an enhancement of stability of active metal species. These preliminary catalytic results

show that isolated iron species are more labile when a significant organic degradation takes place.

3.3. Study of parallel reactions on the phenol photo-degradation

Three additional catalytic runs were carried out using D-2 sample as reference photo-catalyst in order to examine the influence of parallel reactions such as dark-Fenton, degradation mediated by photolysis of H_2O_2 and adsorption phenomenon on the overall degradation of phenol. Table 4 summarizes reaction conditions and catalytic results in terms of TOC and phenol conversions.

Table 4. Experimental results of photo-Fenton blank reactions

Reaction conditions	t_r (min)	X_{TOC} (%)	X_{Phenol}(%)
D-2 catalyst/H₂O₂ **Dark Fenton**	15	3.9	8.5
	30	4.2	-
	75	5.3	-
	150	5.5	-
	240	5.5	51.1
UV/H₂O₂ **Photolysis of oxidant**	15	0.0	7.0
	30	0.0	16.8
	75	4.9	41.0
	150	11.2	61.2
	240	16.5	68.0
UV/D-2 catalyst	15	0.0	0.5
	30	5.3	-
	75	6.4	-
	150	6.6	-
	240	6.5	10.0
UV/H₂O₂/Fe³⁺ **Homogeneous test**	15	0.0	50.0
	30	0.0	86.7
	75	16.5	95.9
	150	19.2	97.7
	240	21.1	98.4

Without lamp but in presence of oxidant and catalyst (dark-Fenton reaction), the TOC removal is less than 6 % after 240 minutes, whereas 51% of phenol is degraded. These results evidence Fenton's reagent in absence of UV light is less active, especially with regard to the carbon mineralization degree. Without any catalyst but with oxidant and UV irradiation, TOC conversion increased up to 17 % and 68% of phenol was removed after 240 minutes of treatment. This noteworthy catalytic performance in absence of catalyst may be attributed to the potential generation of hydroxyl radicals by direct photolysis of the oxidant (reaction 6):

$$H_2O_2 + h\nu \rightarrow 2\ HO^{\bullet} \qquad\qquad (6)$$

With the purpose of measuring a potential adsorption phenomenon of D-2 catalyst in the TOC removal due to its high surface area, an additional experiment was carried out without hydrogen peroxide but in presence of catalyst and UV irradiation. The results shown in Table 4 clearly indicate the negligible contribution of organic adsorption in the pollutant degradation.

Finally, a homogeneous catalytic photo-Fenton run was carried out using $FeCl_3$ as iron source in order to check the contribution of the metallic species homogeneously leached from the catalyst in the overall process. In this way, an appropriate amount of $FeCl_3$ was dissolved in water to attain a reaction media with a concentration of 3 ppm, similar to that leached from the D-2 sample after 240 minutes of reaction. It is clearly evident a lower TOC degradation for the homogeneous run in comparison to the heterogeneous system, especially for initial reaction times. Moreover, it should be

pointed out that the concentration of iron leached from the D-2 sample is much lower for initial reaction times where a significant TOC degradation is observed for the heterogeneous run (see in following Figures 4. a and d).

These results make evident that mineralization of phenol towards carbon dioxide and water by irradiated homogeneous Fenton catalytic systems and UV/H_2O_2 processes may occur along with heterogeneously Fenton photo-assisted reactions, but the remarkable contribution of iron-containing SBA-15 catalyst is undoubtedly demonstrated.

3.4. Comprehensive study of influential parameters in photo-assisted oxidation of phenolic aqueous solutions

As it has been seen in the section 3.2, different catalytic performances in the mineralization of phenolic aqueous solutions have been shown depending on the heterogeneous Fenton-type catalyst. In order to explore further the catalytic behaviour of each photo-catalytic system, special attention has been focused on other parameters such as hydrogen peroxide conversion and pH of the aqueous solution within the course of the reaction and their relationship with the TOC conversion and the iron leaching degree. Figure 4 illustrates the evolution of TOC reduction, hydrogen peroxide conversion, pH solution and iron concentration in the aqueous solution with the reaction time, ascertaining two groups of catalysts: silica-supported iron oxides along with the unsupported commercial hematite (Figures 4 a-d) and ionic iron species incorporated within different silica frameworks (Figures 4 e-h).
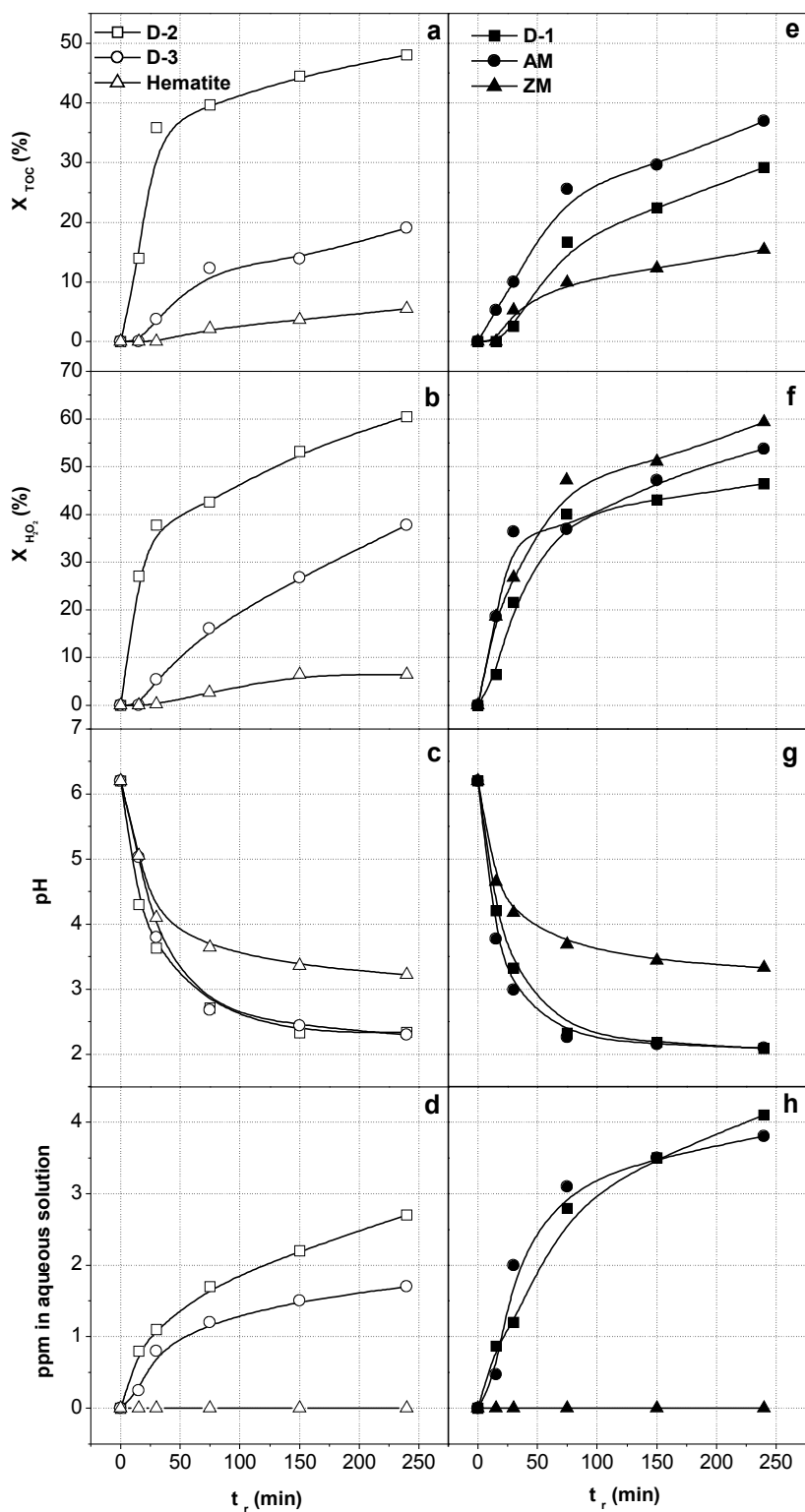
Figure 4. Evolution of influential parameters in the photo-catalytic degradation of phenol using different iron-containing materials: (a and e) TOC removal, (b and f) oxidant consumption, (c and g) pH profiles and (d and h) concentration of iron leaching.

Concerning to silica-supported iron oxides, a remarkable increase of the oxidant conversion is evidenced by D-2 sample for the first minutes of reaction, which is in fairly agreement with a fast TOC degradation rate at that period of time. In contrast, D-3 sample evidences slower oxidant consumption and TOC reduction, and commercial hematite results in an unsuccessful photocatalyst for phenol degradation, exhibiting a low oxidant and TOC conversions. Looking at the pH profiles (Figures 4. c), it is seen a significant decrease of the initial phenolic aqueous pH solution. The decrease of pH solution is commonly attributed to the formation of carboxylic acid as final refractory by-products of the partial oxidation of phenol as reaction proceeds. Furthermore, the radical mechanism involved in a Fenton process according to the reactions outlined in the introduction section with ferrous/ferric ions – note that analogous reactions has been extended to iron heterogeneous catalysts over the solid surface [21] - can also promote a decrease of pH as hydroxyl radicals are formed. It must be pointed out that the stability of catalyst can be affected by the acidic conditions resultant from the reaction. D-2 and D-3 samples showed similar pH profiles for both photocatalytic runs. However, the concentration of leached iron species for D-2 sample is noteworthy higher than that evidenced by D-3. Thus, the different stability shown by these materials is accounted for the distinct nature of the iron species located within the silica matrix (see Table 2). Note that commercial hematite with a higher pH of the aqueous solution during the experiment (over 3.5 most of the reaction time) displays a negligible loss of iron species.

According to the set of low iron-containing catalysts, in which ionic iron species were found within ordered mesoporous SBA-15 (D-1 sample), amorphous xerogel (AM sample) and microporous zeolite (ZM sample), different behaviors can be clearly seen. D-1 and AM photocatalytic systems have yielded similar profiles of pH solution and iron leaching, just exhibiting a slight increase of TOC degradation and hydrogen peroxide consumption for AM sample. Conversely, Fe-silicalite zeolitic material (ZM) displays a surprising high hydrogen peroxide conversion but with a low TOC degradation. These results indicate a non-efficient oxidant decomposition. A plausible explanation could be related to the limited pore diameter of the zeolitic material (5.5 Å) in comparison to the other catalysts. This fact would lead to stronger diffusional hindrances for organic substances as phenol and easier access of oxidant molecules within the microporous zeolitic material. In this sense, decomposition of hydrogen peroxide towards hydroxyl radicals is supposed to happen within the channels, promoting radical scavenging reactions due to the prevailing oxidant presence inside the pores, according to the reaction generally accepted for catalytic systems in excess of oxidant [23]:

$$H_2O_2 + OH^\bullet \rightarrow HO_2^\bullet + H_2O \qquad [7]$$
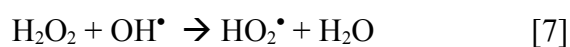
Interestingly, a negligible iron leaching for the ZM photocatalytic run is accompanied with a less acid conditions during the course of reaction (the pH was never lower than 3.5). Taking into account all the tested catalysts, it is noteworthy that the highest stability of hematite and ZM samples agrees with a slighter drop of pH, in comparison to the rest of photocatalysts, which show higher concentrations of iron

leaching with a more significant decrease of pH - values of 2.5-2 (Figure 4 g and h). For Fenton processes homogeneously catalyzed by Fe(III) ions, it has been demonstrated that a pH around 2.8 ensures the presence of iron species in dissolution as Fe (III) and $(Fe(III)(OH)^{2+})$ species, whereas above this point, the concentration of $(Fe(III)(OH)^{2+})$ becomes lower and Fe(III) species precipitate as oxyhydroxides [22]. In this sense, a more important iron leaching as result of partial dissolution of metal heterogeneously supported can be accounted for stronger acidic conditions during the reaction. Likewise, it is also attested that stronger acidic conditions during reaction have promoted a better catalytic performance leading to higher TOC conversions.

Finally, in a process that involves a relatively highly cost reagent, its effective use becomes an important achievement. Figure 5 illustrates the efficiency of hydrogen peroxide as defined in the experimental section versus the TOC conversion at different reaction times with the purpose of assessing an efficient use of the oxidant in combination with a high mineralization degree.
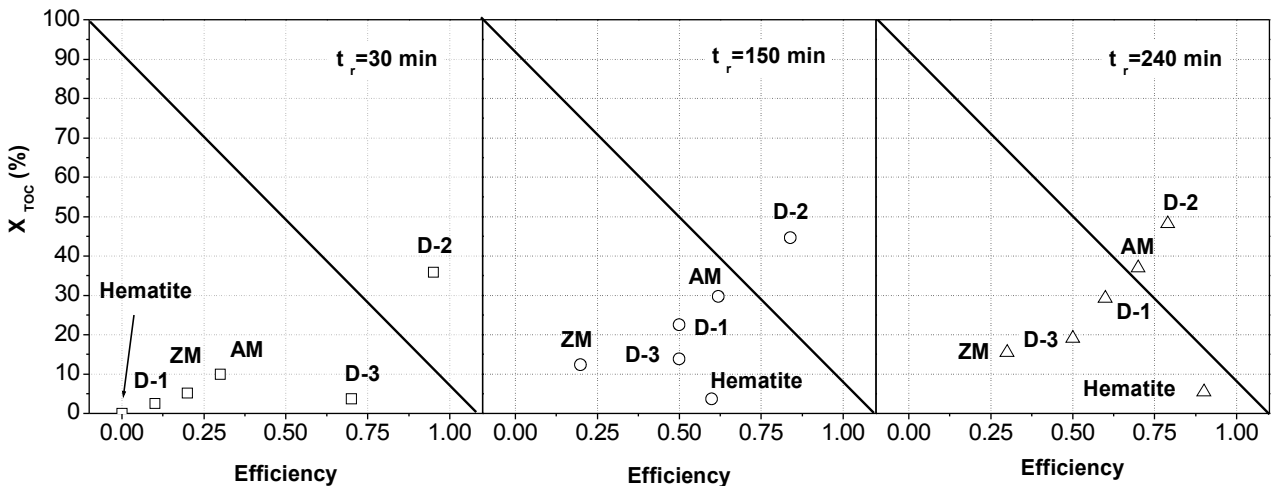
Figure 5. TOC degradation versus oxidant efficiency of iron-containing materials at different reaction times

Interestingly, after 240 minutes of reaction, D-2 sample exhibits the most efficient use of hydrogen peroxide with a nearly 50% of TOC conversion as compared to the rest of catalysts. Conversely, remarkable low oxidant efficiency is displayed for the zeolitic material (ZM sample). This results evidence that either hydrogen peroxide is decomposed to non-powerful oxidant radical species or radical scavenging reactions become dominant in the presence of this photocatalyst as it has been discussed earlier. Surprisingly, the commercial hematite shows a high efficiency coefficient - giving values of 0.85 for reaction times of 240 minutes - although a low TOC removal should be noted by this material. Looking at each photocatalytic system at different reaction times, an increasing of TOC conversion is generally related to higher oxidant efficiency as reaction proceeds.

4. CONCLUSIONS

Activity and stability of iron containing catalysts for treatment of phenolic aqueous solutions by photo-Fenton processes depend on the nature and environment of iron species, which is closely related to the strategy of synthesis. From all tested catalytic systems, it could generally attest that the decrease of pH seems to be related to a better catalytic performance and an increase of iron leaching from the catalyst. These results reveal that the iron resistance to be leached out is influenced by the pH of the reaction media, but the nature and environment of iron species should not be ruled out, playing an important role in the leachibility of each material. Concentration of iron species was not higher than 4 ppm for any of the used catalysts after treatment. It has been

demonstrated that photo-assisted degradation of phenol is mainly due to the heterogeneous role of the catalysts, being other parallel processes poorly relevant. Regarding to iron-containing SBA-15 mesostructured materials, the presence of isolated iron species (D-1 sample) are found more sensitive to be leached out and less active than supported crystalline iron oxide particles (D-2 sample). The later has been shown a promising catalyst for photo-Fenton processes, due to its high activity, stability and efficient use of the oxidant as compared to the rest of tested catalysts.

ACKNOWLEDGEMENTS

REFERENCES

[1] P. R. Gogate, A. B. Pandit, Adv. Environ. Res. 8 (2004) 553.

[2] S. Esplugas, J. Gimenez, S. Contreras, E. Pascual, M. Rodriguez, Wat. Res. 36 (2002) 1034.

[3] L. Plant , M. Jeff, Chem. Eng. (1994) 16.

[4] G. C. Walling, Acc. Chem. Res. 8 (1975), 125.

[5] J. De Laat, H. Gallard, Environ. Sci. Technol. 33 (1999) 2726.

[6] C. Walling, A. Goosen, J. Am. Chem. Soc. 95 (1973) 2987.

[7] V. Nadtochenko, J. Kiwi, Inorg. Chem. 37 (1998) 5233.

[8] M. Rios-Enriquez, N. Shahin, C. Durán-de-Banzúa, J. Lang, E. Oliveiros, S. H. Bossman, A.M. Braun, Solar Energy 77 (2004) 491.

[9] H. E. Feng, S. Xue-you, L. Le-Cheng, J. Environ. Sci. 15 (2003) 351.

[10] J. Feng, X. Hu, P. L. Yue, H. Y. Zhu and G. Q. Lu, Wat. Res. 37 (2003) 3776.

[11] P.L. Yue, J. Y. Feng, X. Hu, Wat. Sci.Technol. 49 (2004) 85.

[12] J. He, X. Tao, W. Ma, J. Zhao, Chem. Lett. (2002) 86.

[13] J. Fernandez, J. Bandara, A. Lopez, P. Buffat, J. Kiwi, Langmuir 15 (1999) 185.

[14] T. Yuranova, O. Enea, E. Mielczarski, J. Mielczarski, P. Albers, J. Kiwi, Appl. Catal. B: Environ. 49 (2004) 39.

[15] F. Martínez, Y. Jhan, G. Stucky, J. L. Sotelo, G. Ovejero, J. A. Melero, Stud. Surf. Sci. Catal. 142 (2002) 1109.

[16] M. A. Uguina, G. Ovejero, R. van Grieken, D. P. Serrano, M. Camacho, Chem. Commun. (1994) 27.

[17] J. A. Melero, G. Calleja, F. Martínez, R. Molina, K. Lazar, Microporous and Mesoporous Mater. 74 (2004) 11.

[18] K. Lazar, G. Calleja, J. A. Melero, F. Martínez and R. Molina, Stud. Surf. Sci. Catal. 154 (2004) 805.

[19] P. Ratnasamy, R. Kumar, Catal. Today 9 (1991) 329.

[20] D.W. Bahnemann. in E. Pelizzetti, M. Schiavello (Eds.), Photochemical conversion and storage of solar energy. Kluver Academic Publishers, Dordrecht, (1991) 251.

[21] M. Noorjahan, V. Durga Kumari, M. Subrahmanyam, L. Panda, Appl. Catal. B: Environ., 57 (2005) 291.

[22] J. J. Pignatello, Environ. Sci. Technol. 26 (1992) 944.

[23] M. Pera-Titus, V. Garcia-Molina, M. A. Banos, J. Gimenez, S. Esplugas, Appl. Catal B: Environ. 123 (2003) 1236.